Application of texture analysis method for mammogram density classification

2017 JINST 12 P07009

(http://iopscience.iop.org/1748-0221/12/07/P07009)

Published by IOP Publishing for Sissa Medialab

Received: *November 22, 2016*
Revised: *May 11, 2017*
Accepted: *June 26, 2017*
Published: *July 6, 2017*

Application of texture analysis method for mammogram density classification

R. Nithya[1] **and B. Santhi**

School of Computing, SASTRA University,
Thanjavur, Tamilnadu, 613402 India

E-mail: nithya.r@mca.sastra.edu

Abstract: Mammographic density is considered a major risk factor for developing breast cancer. This paper proposes an automated approach to classify breast tissue types in digital mammogram. The main objective of the proposed Computer-Aided Diagnosis (CAD) system is to investigate various feature extraction methods and classifiers to improve the diagnostic accuracy in mammogram density classification. Texture analysis methods are used to extract the features from the mammogram. Texture features are extracted by using histogram, Gray Level Co-Occurrence Matrix (GLCM), Gray Level Run Length Matrix (GLRLM), Gray Level Difference Matrix (GLDM), Local Binary Pattern (LBP), Entropy, Discrete Wavelet Transform (DWT), Wavelet Packet Transform (WPT), Gabor transform and trace transform. These extracted features are selected using Analysis of Variance (ANOVA). The features selected by ANOVA are fed into the classifiers to characterize the mammogram into two-class (fatty/dense) and three-class (fatty/glandular/dense) breast density classification. This work has been carried out by using the mini-Mammographic Image Analysis Society (MIAS) database. Five classifiers are employed namely, Artificial Neural Network (ANN), Linear Discriminant Analysis (LDA), Naive Bayes (NB), K-Nearest Neighbor (KNN), and Support Vector Machine (SVM). Experimental results show that ANN provides better performance than LDA, NB, KNN and SVM classifiers. The proposed methodology has achieved 97.5% accuracy for three-class and 99.37% for two-class density classification.

Keywords: Medical-image reconstruction methods and algorithms, computer-aided diagnosis; X-ray mammography and scinto- and MRI-mammography

[1]Corresponding author.

https://doi.org/10.1088/1748-0221/12/07/P07009

2017 JINST 12 P07009

Contents

1 Introduction

The mammogram is considered an efficient screening tool to detect early breast cancer. Mammographic density is a primary risk factor for the development of breast cancer among women [1, 2]. Breast density is measured using mammographic imaging [3]. Recent medical studies have reported

that women with breast density > 75% have a larger risk factor of 4.64 for breast cancer compared to women with breast density < 5% [4]. The breast density is characterized by the amount of glandular tissue in the breast. With the advancement of information technology, Computer-Aided Diagnosis (CAD) system enables us to obtain the highest classification accuracy. CAD system is an automatic or semi-automatic tool designed to help radiologists in mammogram analysis [5]. The digital image processing, artificial intelligence and pattern recognition techniques provide an opportunity for radiologists to enhance their diagnosis with the aid of CAD system. Digital mammography has high resolution and contrast, detects the suspicious lesion. It clearly reveals a lesion, which may not be clinically obvious. Due to this reason, the mammogram is used as the best screening tool by radiologists and many researchers. Breast tissue density classification is an important process in the detection of breast cancer. It is very difficult to identify lesion in the mammogram due to the presence of dense tissue. For this reason, the automatic classification of mammographic density has significance during the process of breast cancer diagnosis. In digital mammogram images, glandular tissue appears as a bright region, whereas fatty tissue appears as a dark region. The presence of higher dense tissue is not an indication of breast cancer but increases the risk of developing breast cancer. The American College of Radiology defines BI-RADS (Breast Imaging-Reporting and Data System) which classifies mammogram into four categories such as fatty (< 25% glandular), fibro-glandular (25–50%), extremely dense (51–75% glandular) and heterogeneously dense (> 75% glandular) [6]. BI-RADS categories are standard approach for density characterization in the mammography. The first two categories are dense, while the last two categories are the higher density groups.

Mammogram density classification is performed in four phases: ROI selection, feature extraction, feature selection and classification. Texture feature extraction is an essential step in the mammogram density classification. The texture features of the mammogram could be extracted using the spatial domain or from a different space [7]. The feature extraction in the spatial domain is based on the first-and second-order statistics. Features extracted from the first-order statistics give information about the gray level distribution of the image, whereas second-order statistics describe information about the relative positions of the various gray levels within the image. Different space by Gabor transform, wavelet transform and trace transform are used to describe the frequency information. These texture features are then fed into the classifiers. Classification is the most important process in the CAD system for breast tissue characterization. Classifiers such as Support Vector Machine (SVM) and Artificial Neural Network (ANN) have performed well in medical image classification. Other classifiers Naive Bayes (NB), Linear Discriminant Analysis (LDA) and K-Nearest Neighbor (KNN) are also employed in this process. In this study, we present an automated approach for breast density classification. The first step of the proposed approach is the selection of Region of Interest (ROI). In the next step, multiple texture features are computed from the digital mammogram. Feature selection and classification are performed in the subsequent steps. Five different classifiers have been compared to evaluate the proposed method using the extracted features. This paper is structured as follows: the summary of the related work is described in section 2. Section 3 provides the methodology of the proposed CAD system. Experimental results are explained in section 4, which are discussed in section 5. Section 6 gives conclusion and future research.

2017 JINST 12 P07009

2 Related work

In recent years, various studies have been done by researchers to classify mammographic breast tissue density. Oliver et al. [8], proposed a method for the breast tissue density using texture and morphological features. The proposed approach was evaluated on the mini- Mammographic Image Analysis Society (MIAS) and Digital Database for Screening Mammography (DDSM) database. Decision tree, KNN, and Bayesian classifiers were used for classification. Subashini et al. [9] presented an automated CAD system for mammogram density classification using first-order statistical histogram features. In their study, ROI was extracted by excluding the pectoral muscle, artifacts, and background from the mammogram. SVM was used as a classifier to characterize mammogram into three categories (fatty, glandular and dense). Mustra et al. [10] proposed an approach for breast tissue density classification using texture features. They presented two different classification tasks: four-class classification problem based on the BIRADS categories and three-class (fatty, glandular and dense) density classification. KNN was used as a classifier to classify the mammography images of the mini-MIAS and DDSM dataset. Vallez et al. [11] proposed automated CAD system for breast density classification using texture features. They proposed method was tested on the MIAS dataset and full-field digital mammogram dataset for BI-RADS density classification. In their work, a novel weighted voting tree classifier was used for breast tissue classification. Sharma et al. [12] developed a system based on texture features for automated breast density classification. Their ROI was manually selected from the mammogram in such a way that ROI included breast tissue only excluding the pectoral muscle. The mini-MIAS database was employed to assess the performance of the proposed system. In their approach, Correlation Feature Selection (CFS) was applied to select the redundant features that differentiate between fatty and dense tissue. Sequential Minimal Optimization (SMO) was used as a classifier. In their study, the mammogram was classified into two categories of fatty and dense. Arefan et al. [13] classified the mammogram into three categories of fatty, glandular and dense. In their study, ROI was an entire breast region, excluding the pectoral muscle. They used mammogram images from the mini-MIAS database. ANN classifier was used to classify the mammogram images. Abdel-Nasser et al. [14] proposed uniform local directional pattern as a texture descriptor to perform two-class (fatty/dense) and three-class (fatty/dense/glandular) breast tissue density classification. They used SVM classifier to evaluate the proposed method on the mini-MIAS database. The method proposed in Sharma et al. [15], was used to classify mammogram into a fatty and dense tissue. Texture features were extracted from each manually extracted ROI that contains only breast tissue. The extracted texture features were classified using k-NN classifier. Their proposed method was evaluated on the mini-MIAS database.

3 Methodology

The proposed CAD system for mammography density classification consists of four phases: selection of ROI, feature extraction, feature selection and classification. Image processing and data mining techniques were used in this proposed methodology. The overview of the proposed CAD system is shown in figure 1.

2017 JINST 12 P07009

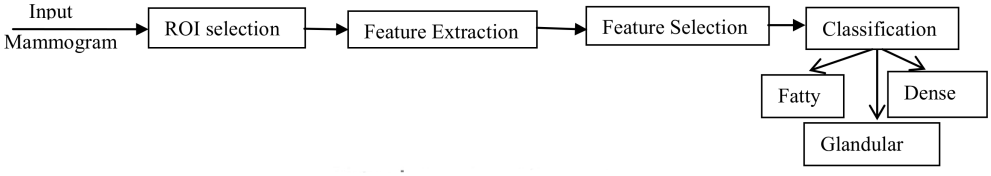

Figure 1. Overview of CAD system.

3.1 Dataset

The mammograms used in this work were obtained from the Mini-MIAS database. The web page for the MIAS resource is located at http://peipa.essex.ac.uk/info/mias.html. Mammogram is an x-ray of the breast. The MIAS database contains 322 left and right breast images of 161 patients [16]. The mammogram was acquired in the Medio-Lateral Oblique (MLO) view. These images were categorized into three groups: fatty, glandular and dense. All the images were 1024×1024 pixels in size. The MIAS database is a public database, made freely available on the internet. 240 mammograms were used in this work. There were 80 fatty, 80 glandular and 80 dense mammograms. Breast density type for each mammogram is provided by experienced radiologist [17].

3.2 ROI selection

ROI selection was employed to segment the interested region of the mammogram. The primary objective of this ROI selection is to identify the mammogram region that contains dense tissue. During the ROI selection, the dense region was selected based on the highest intensity point and this extracted region was used in feature extraction. The selection of ROI is the dense region of the mammogram. Every ROI size is 256×256 pixel. A total of 240 ROI images were used in this study. Extracted ROI contains breast tissue only, excluding label, background and pectoral muscle region. The extracted ROI of fatty, glandular and dense mammograms are depicted in figure 2.

(a) Fatty (b) Glandular (c) Dense

Figure 2. Sample ROIs from the mammogram.

3.3 Feature extraction

Texture features were extracted in order to classify the mammogram into three density classes, namely fatty, glandular and dense. Texture features are the most commonly used features of a

breast cancer of the CAD system. The CAD system was used to classify the mammogram based on the extracted features. Feature extraction is an essential part of the classification process. Pattern recognition depends on the extracted features that classify the object of interest. In the mammogram gray scale image, the pixel values are different among fatty, glandular, and dense tissue pattern. The following feature extraction methods provide information about gray level distribution in the mammogram images. It can be useful for density classification.

3.3.1 Histogram features

First-order statistics features were computed from the histogram of the mammogram image. The histogram is represented by a graph. It provides information about gray level distribution in the mammogram image. For gray scale image, the histogram graph with an x coordinate range from 0 to 255 and a y coordinate represents the corresponding pixel count [18]. From the histogram, six statistical measures were extracted, which include mean, entropy, standard deviation, uniformity, smoothness and third moment. The advantage of first-order statistics is simple and it provides an effective description of the gray level distribution. The limitation is very sensitive to noise.

- Mean (m) = $\sum_{i=0}^{L-1} z_i p(z_i)$
- Standard deviation (σ) = $\sqrt{\sigma}^2$
- Variance (σ^2) = $\sum_{i=0}^{L-1} (z_i - m)^2 p(z_i)$
- Smoothness = $1 - \frac{1}{(1+\sigma^2)}$
- Third moment = $\sum_{i=0}^{L-1} (z_i - m)^3 p(z_i)$
- Uniformity = $\sum_{i=0}^{L-1} p^2(z_i)$
- Entropy = $-\sum_{i=0}^{L-1} p(z_i) log_2 p(z_i)$

where L is the total number of different intensity pixels, z_i is a pixel intensity, $p(z_i)$ is normalized histogram, with $i = 0, 1, 2, \ldots, L-1$.

3.3.2 Gray Level Co-Occurrence Matrix (GLCM)

GLCM was used for extracting second-order statistics texture information from images. In GLCM, each element $P(i, j|d, \theta)$ is described as the probability of gray levels i and j occurrence separated by distance d and direction θ. Here $P(i, j)$ is the (i, j)th entry in the normalized histogram. GLCM features were calculated in four distances (1, 2, 3, and 4) and four directions which are 0°, 45°, 90°, 135°. The choice of θ based on every pixel which has neighbours at θ = 0°, 45°, 90° and 135°. 18 features were extracted from GLCM. These features are as follows: autocorrelation, correlation, contrast, cluster shade, cluster prominence, dissimilarity, entropy, sum entropy, difference entropy, energy, sum average, maximum probability, homogeneity, sum of squares variance, sum variance, information measure of correlation1, inverse difference moment and information measure of correlation2 [19, 20]. GLCM provides more number of features than histogram. The disadvantage of this approach is its high computational cost.

- Contrast = $\sum_{i=0}^{G-1}\sum_{j=0}^{G-1} P(i,j)(i-j)^2$
- Correlation = $\sum_{i=0}^{G-1}\sum_{j=0}^{G-1} P(i,j)\times(i\times j)-(\mu_x\times\mu_y)/\sigma_x\sigma_y$
- Cluster prominence = $\sum_{i=0}^{G-1}\sum_{j=0}^{G-1} P(i,j)(i+j-\mu_x-\mu_y)^4$
- Autocorrelation = $\sum_{i=0}^{G-1}\sum_{j=0}^{G-1} (ij)\,P(i,j)$
- Cluster shade = $\sum_{i=0}^{G-1}\sum_{j=0}^{G-1} P(i,j)(i+j-\mu_x-\mu_y)^3$
- Dissimilarity = $\sum_{i=0}^{G-1}\sum_{j=0}^{G-1} |i-j|P(i,j)$
- Energy = $\sum_{i=0}^{G-1}\sum_{j=0}^{G-1} P(i,j)^2$
- Entropy = $-\sum_{i=0}^{G-1}\sum_{j=0}^{G-1} P(i,j)log(P(i,j))$
- Homogeneity = $\sum_{i=0}^{G-1}\sum_{j=0}^{G-1} \frac{P(i,j)}{1+|i-j|}$
- Maximum probability = $\max(i,j)\,P(ij)$
- Sum of squares: variance = $\sum_{i=0}^{G-1}\sum_{j=0}^{G-1} P(i,j)\,(i-\mu)^2$
- Sum average = $\sum_{i=0}^{2G-2} iP_{x+y}(i)$
- Sum entropy (se) = $-\sum_{i=0}^{2G-2} P_{x+y}(i)\log(P_{x+y}(i))$
- Sum variance = $\sum_{i=0}^{2G-2}(i-se)^2\,p_{x+y}(i)$
- Difference entropy = $-\sum_{i=0}^{G-1} P_{x-y}(i)\,log(P_{x-y}(i))$
- Information measure of correlation1 = $\frac{\mathrm{HXY-HXY1}}{max\{\mathrm{HX,HY}\}}$
- Information measure of correlation2 = $\sqrt{(1-\exp[-2.0(\mathrm{HXY2}-\mathrm{HXY})]}$
- Inverse difference moment normalized = $\sum_{i=0}^{G-1}\sum_{i=0}^{G-1} \frac{P(i,j)}{1+|i-j|^2/G^2}$

where G is the total number of different gray values in the image. P is the computed GLCM. μ is the mean of the entire normalized GLCM. Mean of P_x and P_y are μ_x and μ_y. Standard deviations of P_x and P_y are σ_x and σ_y. HX and HY are the entropies for P_x and P_y.

$$P_x(i) = \sum_{j=0}^{G-1} P(i,j)$$
$$P_y(j) = \sum_{i=0}^{G-1} P(i,j)$$
$$\mu = \sum_{i,j=0}^{G-1} iP(i,j)$$

2017 JINST 12 P07009

$$\mu_x = \sum_{i=0}^{G-1} i \sum_{j=0}^{G-1} P(i,j) = \sum_{i=0}^{G-1} iP_x(i)$$

$$\mu_y = \sum_{i=0}^{G-1} \sum_{j=0}^{G-1} jP(i,j) = \sum_{j=0}^{G-1} jP_y(j)$$

$$\sigma_x^2 = \sum_{i=0}^{G-1} (i-\mu_x)^2 \sum_{j=0}^{G-1} P(i,j) = \sum_{i=0}^{G-1} (P_x(i)-\mu_x(i))^2$$

$$\sigma_y^2 = \sum_{j=0}^{G-1} (j-\mu_y)^2 \sum_{i=0}^{G-1} P(i,j) = \sum_{j=0}^{G-1} (P_y(j)-\mu_y(j))^2$$

$$P_{x+y}(k) = \sum_{i=0}^{G-1} \sum_{j=0}^{G-1} P(i,j) \quad i+j=k \qquad \text{for} \quad k = 0,1,\ldots,2(G-1)$$

$$P_{x-y}(k) = \sum_{i=0}^{G-1} \sum_{j=0}^{G-1} P(i,j) \quad i-j=k \qquad \text{for} \quad k = 0,1,\ldots,G-1$$

$$HX = -\sum_{i=0}^{G-1} P_x(i) \log_2 P_x(i)$$

$$HY = -\sum_{j=0}^{G-1} P_y(j) \log_2 P_y(j)$$

$$HXY = -\sum_{i,j=0}^{G-1} P(i,j) \log_2 P(i,j)$$

$$HXY1 = -\sum_{i,j=0}^{G-1} P(i,j) \log_2 (P_x(i) P_y(i))$$

$$HXY2 = -\sum_{i,j=0}^{G-1} P_x(i) P_y(i) \log_2 (P(i) P(i)$$

3.3.3 Gray Level Run Length Matrix (GLRLM)

GLRLM is computed as the total number of adjacent pixels that have the specific gray value in a given direction θ. The choice of θ is similar to GLCM. Five texture features were extracted using the GLRLM: long run emphasis, run-length non-uniformity, short run emphasis, run percentage, and gray level non-uniformity [21]. The element $P(i, j|\theta)$ of GLRLM describes the total number of existences of runs of length j for gray level i in the angle θ direction. For the GLRLM, the values used for θ were 0°, 45°, 90°, and 135°. The choice of θ is similar to GLCM. GLRLM gives information about the spatial distribution of gray level runs. The advantage of this approach is that it can preserve much of the texture information in run-length matrices. The disadvantage of this approach is that many of these features are highly correlated with each other.

- Short run emphasis = $\frac{\sum_{i=1}^{N_g} \sum_{j=1}^{N_r} P(i,j)/j^2}{\sum_{i=1}^{N_g} \sum_{j=1}^{N_r} P(i,j)}$

2017 JINST 12 P07009

- Long run emphasis = $\frac{\sum_{i=1}^{N_g}\sum_{j=1}^{N_r} j^2 P(i,j)}{\sum_{i=1}^{N_g}\sum_{j=1}^{N_r} P(i,j)}$
- Gray-level non-uniformity = $\frac{\sum_{i=1}^{N_g}\left[\sum_{j=1}^{N_r} P(i,j)\right]^2}{\sum_{i=1}^{N_g}\sum_{j=1}^{N_r} P(i,j)}$
- Run-length non-uniformity = $\frac{\sum_{j=1}^{N_r}\left[\sum_{i=1}^{N_g} P(i,j)\right]^2}{\sum_{i=1}^{N_g}\sum_{j=1}^{N_r} P(i,j)}$
- Run percentage = $\frac{\sum_{i=1}^{N_g}\sum_{j=1}^{N_r} P(i,j)}{\sum_{i=1}^{N_g}\sum_{j=1}^{N_r} P}$

where N_g is the maximum gray-level, N_r Is the total number of different lengths that occurs and P is the total number of image pixel point.

3.3.4 Gray Level Difference Matrix (GLDM)

GLDM is computed as the absolute difference in gray level of two pixels. Let I(x, y) be the image pixel intensity. Then for any given displacement= $(\Delta x, \Delta y)$, the absolute difference between a pair of gray level is estimated as

$$I_\delta(xy) = |I(xy) - I(x + \Delta x y + \Delta y)|$$

The probability density function $D(i|\delta)$ that two pixels with distance d is defined by the angle θ, i is the gray level difference and $\delta = (d, \theta) \cdot D(i|\delta)$ was computed for four directions θ: 0°, 45°, 90°, and 135°. Four texture features were extracted using $D(i|\delta)$: contrast, entropy, mean and angular second moment [21, 22]. The advantage of these features is that they are robust to differences in the four directions. However, the calculation of feature is computationally costly.

- Contrast = $\sum_i i^2 D(i|\delta)$
- Mean = $\sum_i iD(i|\delta)$
- Entropy = $-\sum_i D(i|\delta) \log D(i|\delta)$
- Angular Second moment = $\sum_i D(i|\delta)^2$

3.3.5 Entropy

The randomness of image pixels is determined by entropy measure. Four entropy measures such as Shannon, Renyi, Kapur, and Yagor were used to measure the randomness of the intensity distribution of the mammogram images. Entropy measures showed an advantage in computational efficiency. Considering the image I(xy) , have N_i $(i = 0, 1, 2, 3, 4, \ldots, L-1)$ distinct intensity values [23, 24]. The normalized histogram of the given image $I(x, y)$ having size of $A \times B$ can be computed as

$$F_i = \frac{N_i}{A \times B}$$

where A and B are rows and columns of the image respectively.

2017 JINST 12 P07009

Shannon Entropy can be calculated by

$$S_n = -\sum_{i=0}^{L-1} F_i \log_2 F_i$$

Renyi's entropy can be calculated by

$$R = \frac{1}{1-\alpha} \log_2 \sum_{i=0}^{L-1} F_i^{\alpha}$$

where α is diversity index. Here $\alpha = 3$.

Kapur's entropy can be calculated by

$$K_\alpha = \frac{1}{\beta - \alpha} \log_2 \frac{\sum_{i=0}^{L-1} F_i^{\alpha}}{\sum_{i=0}^{L-1} F_i^{\beta}}$$

where α and β is diversity indices. Here $\beta = 0.7$, $\alpha = 0.5$.

Yager's entropy can be calculated by

$$Y = \frac{\sum_{i=0}^{L-1} |2F_i - 1|}{|A \times B|}$$

3.3.6 Local Binary Pattern (LBP)

LBP effectively combines characteristics of statistical and structural texture analysis. The LBP is a powerful method for medical image classification. LBP is a textural measure of local neighbourhood. For each pixel, LBP measure uses a circular neighbourhood for given radius. The image LBP code can be calculated as follows: P is the number of pixels selected on the circumference of the circle with radius R. Let g_p, $p = 0, \ldots, p-1$ be the pixel intensity value and g_c be the center pixel intensity value. P points are changed to a circular bit-stream of 0s and 1s based on whether the gray value of the pixel is greater than or less than the centre pixel gray value. Let U be the number of spatial bitwise 0/1 transitions.

$$\mathrm{LBP}_{P,R}(x) = \begin{cases} \sum_{P=0}^{P-1} s(g_p - g_c) & \text{if} \quad U(x) \leq 2 \\ P+1, & \text{otherwise} \end{cases} \tag{3.1}$$

$$s(x) = \begin{cases} 1, & x \geq 0 \\ 0, & x < 0 \end{cases} \tag{3.2}$$

where P is the pixel count, g_i is the pixel intensity and g_c is the centre pixel intensity.

Three LBP images were obtained using the radius ($R = 1$, 2 and 3 with the pixel count $P = 8$ [25]. The mean (LBP1-LBP3), standard deviation (LBP4-LBP6), and energy (LBP7-LBP9) of three LBP images were used as feature descriptors. The advantage of the LBP is the efficiency of analyzing features. The limitation is that it cannot capture features in a large scale.

2017 JINST 12 P07009

3.3.7 Gabor transform

Gabor filter is applied to extract the texture features by analyzing the frequency domain properties of the image. It has the ability to perform both in frequency and spatial domain. Gabor filter is obtained by multiplying a sinusoidal plane of a particular frequency with a Gaussian envelope [26, 27]. A Gabor filter bank consists of multiple Gabor filters with different parameters (orientation and frequency). Sixteen Gabor filtered images were obtained for each mammogram. A total of 16 Gabor filtered images were obtained using 4 orientations, θ (0°, 45°, 90° and 135°) and four frequencies (0.2, 0.3, 0.4 and 0.5). The mean (Gabor1-Gabor16) and standard deviation (Gabor17-Gabor32) features were extracted from the 16 Gabor filtered images. The advantage of the Gabor transform is that it describes the property of both frequency and spatial domain. The disadvantage is the high computational cost due to the dimension of feature vector which is very long.

3.3.8 Wavelet Texture Descriptors

Multiresolution approaches such as wavelet packet transform and discrete wavelet transform were employed for feature extraction in the transform domain. Discrete Wavelet Transform (DWT) and Wavelet Packet Transform (WPT) reveal that mean and standard deviation features are useful for medical image classification. In this study, mean and standard deviation were calculated from the sub-band images generated using 2D-DWT and 2D-WPT. The wavelet basis function used here was Daubechies-1. By third-level decomposition, ten sub band images were obtained using 2D-DWT. Twenty features were computed based on the statistical mean (DWT1-DWT10) and standard deviation (DWT11-DWT20) from the ten sub-bands images. By second-level decomposition, sixteen sub band images were obtained using 2D-WPT. Using 2D-WPT, 32 features were computed based on the statistical mean (WPT1-WPT16) and standard deviation (WPT17-WPT32) using sixteen sub-band images. DWT can be performed by the images are sent through a sequence of down-sampling low-pass and high-pass filters. The image is decomposed into LL, HH, HL, and LH (Low-Low, High-High, High-Low, and Low-High) sub-band images [28]. DWT computes the approximation coefficients LL and details coefficients matrices LH, HL, and HH obtained by a wavelet decomposition of the input image. The WPT is an extension of DWT. In WPT, the images were sent through more filters than DWT. The WPT calculates each level by passing both approximation and detail coefficients to Quadrature Mirror Filters (QMF), whereas DWT passes only the previous approximation coefficients sent through QMP to generate a full binary tree [29]. The advantage of wavelet based sub-band feature extraction is that it provides more distinct features. The disadvantage of this approach is that it is computationally intensive.

3.3.9 Trace transform

The trace transform is similar to the Radon transform. Trace functionals were used to extract features which are invariant to transformation such as translation, rotation and scaling. The trace transform is obtained by applying a trace functional T along the line tracing the input image. Several functionals were developed to extract features from mammograms [30]. A list of functionals used in mammogram feature extraction is shown in table 1. T, the trace functional, is applied along lines tracing the original image in order to transform the image into the (φ, p, t) parameter space. φ is the direction, p is the distance of the centre of the image from the tracing line and t is the sampling

Table 1. Trace functionals.

S.No	Trace Functional
T1	$\sum_{i=1}^{N} x_i$
T2	$\sum_{i=1}^{N} i x_i$
T3	$\frac{1}{N}\sqrt{\sum_{i=1}^{N}(x_i - \hat{x})^2}$
T4	$\sqrt{\sum_{i=1}^{N} x_i^2}$
T5	$\sum_{i=1}^{N-1} \lvert x_{i+1} - x_i \rvert$
T6	$\sum_{i=1}^{N-1} \lvert x_{i+1} - x_i \rvert^2$
T7	$\sum_{i=1}^{N-1} \lvert x_{i+1} - x_i \rvert^3$
T8	$\frac{1}{N}\sqrt{\sum_{i=4}^{N-3}(x_i - \hat{x})^2}$
T9	$\sum_{i=4}^{N-3} i x_i$
T10	$\sum_{i=4}^{N-3}(-\hat{x})^2$

intervals of tracing lines. In this work, we have chosen $\varphi = 1$ to 180°, $t = 0.5$ and $p = 2$. The advantage of trace transform is that it produces a more number of features with spatial domain but implementation is complicated and time consuming.

In trace functionals, x_i is the intensity value of the image at point i along the tracing line and N is the total number of points considered along the tracing line.

3.4 Feature selection

The feature selection method was employed to enhance the performance of the classifier. The objective of feature selection method is to reduce a total number of features to achieve highest classification accuracy and also to minimize the computational complexity. Various features were computed from the mammogram images. Extracted features may contain some irrelevant or redundant features. The uses of all the features degrade the performance of the classifier as well as increase the computational time. So the selection of a relevant feature is essential for the classification task. The accuracy of the system depends on the relevant feature selection. Feature selection methods like analysis of variance (ANOVA) select the useful and unique features.

3.4.1 Analysis of variance (ANOVA)

Significant features were selected using the ANOVA test. Feature ranking methods like ANOVA select the useful features. In this work, one-way ANOVA test was used. The variation of a feature within the group and the variation between the groups were calculated. If the variation of a feature between the group is higher than the within the group, the feature is considered to be statistically significant [31]. Pearson's correlation coefficient was used for finding the correlation between features. The Pearson correlation was performed by generating the correlation matrix. The ANOVA test result is the p-value and F-value. The ratio of the mean squared error is the F-value. A low p-value (< 0.0001) shows that the means of individual groups are independent. Features were

ranked using the F-value. The feature with highest F-value was ranked highest as they efficiently characterize between different classes. p-value was computed based on F-value and degrees of freedom using statistical table.

3.5 Classification

Classifier selection is an important step for computer-aided breast density classification. In this work, selected texture features were fed into classifiers for the automated classification of mammogram into a fatty, glandular and dance classes.

3.5.1 Artificial Neural Network (ANN)

ANN is the commonly used classifier in medical image classification. The neural network classifier comprises two phases, namely training and testing. The neural network was trained for the target output based on the input values during the training phase. In the testing phase, an unknown sample was predicted using the trained network. ANN had three-layers: an input layer with 31 nodes, a hidden layer with N nodes, and an output layer with one node [32]. The nodes were interconnected by weights and information propagated from one layer to the next through a sigmoid activation function. ANN has been trained with adaptive learning rate and momentum. In order to find the appropriate number of hidden neurons, and the values of learning rate and momentum, trial-and-error process has been applied. The weight between input and hidden layer, hidden and the output layer was assigned, and then the output was calculated. The network learns by adjusting the weight between nodes. The neural network output was determined by Mean Square Error (MSE). The MSE was calculated as the difference between the target output and network output. The input and output values were normalized between 0 and 1 [33]. The advantage of ANN is that it is easy to use and implement. The limitation is that it requires huge processing time if neural network is large.

3.5.2 k-Nearest Neighbour (KNN)

The KNN classifier consists of the assignment of an unknown sample class using the closest k samples found in the training set. In this method, the contribution of each of the k neighbor weight was estimated based on its distance from the unknown sample giving highest weight to closer neighbors. The Euclidean distance was computed between the unknown sample and each of all the k neighbors in the training set [34]. The sum of votes was calculated for each class and then unknown sample class was determined by the class of the highest sum of votes. The performance of KNN classifier can be very sensitive to the choice of k neighbors. In this work, we used the K value between 2 to 5. The maximum classification accuracy obtained for $K = 3$. KNN classifier is simple to understand and easy to implement. The disadvantage of KNN is that it is very sensitive to redundant or irrelevant features.

3.5.3 Support Vector Machine (SVM)

The SVM classifier is a supervised learning method used for regression analysis and pattern recognition. It provides fast learning capacity for the large feature set. The classification is based on the concept of a hyper plane that separates the classes with maximum margin. The best hyper plane is determined by maximizing the distance between the training samples and the hyper plane.

2017 JINST 12 P07009

The training samples that determine the hyper plane are called as support vectors [35]. Both linear and non-linear classification can be performed using the SVM. The kernel functions used in SVM are polynomial, quadratic, Gaussian and Radial Basis Function (RBF). In this work, RBF kernel function was used. SVM performs multiclass classification by combining two class SVMs. The advantage of SVM is that it works well in high dimensional feature space. The disadvantage of SVM classifier is that its appropriate selections of kernel function and its parameters.

3.5.4 Naive Bayes (NB)

The Bayesian classifier is a statistical method as well as a supervised learning method for classification. Naive Bayes classifier is the probabilistic induction method based on Bayes theorem. The naïve Bayes classifier is a simplified Bayesian probability model. It calculates the posterior probability that an unknown sample belongs to a certain class [36, 37]. NB classifier assumes that the value of the attribute on a given class is independent of other attribute values. This assumption is known as class conditional independence. The Naive Bayes used was the Gaussian Naive Bayes. The advantage of this classifier is that it is simple to implement, but it requires a large number of training to obtain high accuracy.

3.5.5 Linear discriminant analysis (LDA)

LDA is a supervised learning method based on the statistical approach for classification and feature reduction. The basic concept of LDA is to determine the linear combination of features that separate different classes of data. In this method, within class and between class scatter matrices determine the efficiency of the classification. LDA finds the discriminant dimension in which the ratio of between-class and within-class variance is maximized [37]. This method considers both between-class differences and within-class similarities. LDA is under the homoscedasticity assumption that the class covariance is identical. LDA is a well-known statistical technique that works well in pattern classification. The limitation is that it assumes that the underlying model is a multivariate normal distribution.

3.5.6 Evaluation measures

The performance of the classifiers was evaluated using the ten-fold cross validation. The data sample was split into ten equal subsets, with each subset containing equal number of images from each class. In the first fold, classifiers were trained with the nine subsets and the other one subset used to test the classifier [38]. This process was repeated nine-fold using a different test subset. The performance of the classifiers was evaluated by classification accuracy, specificity, and sensitivity for every fold. The average of all the folds gives the actual classification accuracy, specificity and sensitivity. Sensitivity measures the proportion of positive cases, which are correctly classified while specificity measures the proportion of negative cases, which are correctly classified. Classification accuracy measures the percentage of positive and negative cases, which are correctly classified.

- Accuracy = $\frac{\text{TP+TN}}{\text{(TP+FN+TN+FP)}} \times 100\%$
- Sensitivity = $\frac{\text{TP}}{\text{(TP+FN)}} \times 100\%$
- Specificity = $\frac{\text{TN}}{\text{(TN+FP)}} \times 100\%$

where:

- TP (True Positive) — Number of mammogram images correctly categorized as a given class.
- FP (False Positive) — Number of mammogram images incorrectly categorized as a given class.
- TN (True Negative) — Number of mammogram images correctly categorized as not a given class.
- FN (False Negative) — Number of mammogram images incorrectly categorized as not a given class.

4 Experimental results

The mammogram images were obtained from the mini-MIAS database. Totally, we extracted 140 texture features from each mammogram. The features such as Histogram (6), GLCM (18), and GLDM (4), GLRLM (5), and LBP (9), entropy (4), Gabor (32), wavelet (52) and trace transform (10) were extracted for three classes. We extracted 140 features using the above-mentioned methods and 31 features were found that efficiently discriminating between three density classes using the ANOVA analysis. Multiple texture features were extracted from fatty, glandular and dense classes provided sufficient discrimination between classes with the P-value <0.0001. The discrimination efficiency of the extracted features between three classes was determined by p-value and these features were ranked by F-value. Table 2 shows the selected feature (mean and Standard Deviation (SD)) for the three classes of mammogram used in this work. The result satisfies the ANOVA assumptions on independence, normality and homoscedasticity. All features were tested for normality and homoscedasticity. Two different experiments were tested with the mini-MIAS database: fatty/glandular/dense and fatty/dense tissue classifications. In the first experiment, mammogram images were classified into three groups according to classification of MIAS database. In the second experiment, mammogram images were classified into two groups according to low or high density. In two class classification, glandular and dense mammograms were grouped into the dense class. In this work, we have employed five classifiers to evaluate the performance of the selected features. All the selected features were fed into ANN, KNN, NB, LDA and SVM classifier to classify the breast density classes. These 5 supervised learning classifiers were proven effective in medical image classification. The classifiers were trained and tested for 10-fold to obtain better accuracy. In each fold, we have obtained different results for accuracy, sensitivity and specificity due to different random samples of 240 images. The average of all folds gives the classification accuracy, specificity, and sensitivity for all the classifiers. For the two categories, the obtained classification accuracy is 99.37%. The highest classification accuracy for three-class is 97.5%. It has been obtained using the ANN classifier. Tables 3 and 4 show the performance measures of the classifiers for fatty/dense and fatty/glandular/dense tissue classification. It can be observed from figure 3, that the classification accuracy of the selected features is comparatively better than all features. There were significant improvements in the accuracy of the classifiers using the selected features. The classification accuracy of fatty/glandular/dense is lower than the

2017 JINST 12 P07009

fatty/dense classification rate due to the glandular class. It can be observed from tables 3 and 4 that ANN classifier achieved highest classification accuracy using the selected features.

5 Discussion

Various studies have been proposed in the automated mammographic density classification. This work proposes a method for characterization of breast tissue density using multiple texture features. In this study, we have performed the classification of two and three classes of mammogram images. We used 240 mammogram images for breast tissue characterization based on 140 texture features extracted from the mammogram. The extracted features were used to classify the fatty, glandular and dense mammogram. Classifications of fatty, glandular and dense classes were based on the selected features. The proposed method enables in classifying the fatty and dense mammograms with 99.37% accuracy; fatty, dense and glandular mammogram with 97.5% accuracy. The novelty of this work is the feature extraction process. In the feature extraction step, multiple statistical texture features were extracted from the mammogram images. To validate the proposed method, we have compared five classifiers such as ANN, SVM, LDA, NB, and K-NN. The obtained classification accuracy based on all features is in the range of 75–90% as shown in figure 3. The ANOVA analysis reduced the feature set to 31 features and significantly improved the classification accuracy in the range of 91–97%. As described in experimental results, highest classification results have been obtained by the ANN classifier compared to other classifiers such as SVM, LDA, KNN, and NB. LDA and SVM classifiers produced the second best classification results. ANN provides high accuracy, sensitivity and specificity for three-class and two-class classification. ANN, SVM, LDA, KNN and NB in selected features have higher accuracy than all features. It is seen from table 5 that various studies have been proposed for mammographic three and two category density classification. The proposed work is compared with the related publications in the literature. In [11], the authors classified mammogram into four categories of BI-RADS. They obtained better accuracy of 99.8% and sensitivity of 99.9% for four class classification according to BI-RADS. However, the trace transform and DWT based features have not been used in density classification so far. To the best of our knowledge, this work is the first of its kind using this method for mammographic density classification. In this work, we have used the combination of several texture features that obtained better accuracy in density classification. Based on the experimental results, we conclude that texture features can well characterize breast tissues in digital mammograms.

6 Conclusion

This work proposes an automated approach to classify breast tissue density classes using the multiple texture features. To select the optimal features from the multiple features, ANOVA analysis is used. The efficiency of the proposed system is tested using five different supervised learning classifiers with selected features. The proposed CAD system obtained classification accuracy of 99.37% for two categories and 97.5% accuracy for three category density classification. Our proposed CAD system is helpful for radiologists to perform precise and faster diagnosis. The proposed system can further be extended to classify four categories (fatty, glandular, heterogeneously dense and extremely dense) of breast density based on BI-RADS.

2017 JINST 12 P07009

Table 2. Results of selected features that had a p-value < 0.0001 for fatty, glandular and dense classes.

Feature extraction methods	Features	Fatty		Dense		Gland		p-value	F-value	Rank
		Mean	SD	Mean	SD	Mean	SD			
Histogram	Mean	118.47	24.68	140.18	16.26	193.82	19.86	0.00E+00	284.83	4
GLCM	Autocorrelation	19.29	5.85	24.63	4.10	40.56	6.40	0.00E+00	319.23	2
	Maximum probability	0.65	0.21	0.48	0.13	0.66	0.15	1.26E−11	27.96	27
	Sum of squares variance	19.16	5.84	24.54	4.07	40.38	6.38	0.00E+00	319.73	1
	Sum average	8.55	1.40	9.71	0.90	12.63	1.05	0.00E+00	272.53	6
	Sum variance	62.48	26.20	73.34	17.01	139.74	30.23	0.00E+00	222.23	8
	Contrast	47.93	30.50	65.54	13.24	41.03	17.86	1.29E−11	27.93	28
	Difference entropy	0.22	0.11	0.29	0.04	0.20	0.07	2.97E−11	26.90	29
GLRLM	Long Run Emphasis	19.34	5.84	24.65	4.12	40.60	6.39	0.00E+00	319.21	3
LBP	LBP2	0.09	0.01	0.09	0.01	0.06	0.02	0.00E+00	140.69	13
	LBP4	3.07	0.34	3.94	0.35	3.50	0.52	0.00E+00	88.97	20
	LBP6	0.47	0.01	0.46	0.01	0.43	0.03	0.00E+00	120.04	15
	LBP8	0.43	0.05	0.37	0.04	0.30	0.05	0.00E+00	151.52	11
	LBP9	0.49	0.01	0.48	0.01	0.45	0.03	0.00E+00	98.47	18
Gabor	GA1	2.29	0.57	2.57	0.50	3.46	0.70	0.00E+00	83.99	22
	GA11	6.07	1.15	6.68	0.97	9.33	1.20	0.00E+00	193.96	10
	GA12	0.52	0.13	0.58	0.09	0.80	0.11	0.00E+00	146.75	12
	GA31	8.94	1.68	9.84	1.44	13.76	1.76	0.00E+00	197.57	9
Trace	T1	537.16	240.9	598.48	239.3	803.78	214.4	5.39E−12	29.01	25
	T2	1651.7	685.0	1748.5	682.5	2363.9	682.8	8.89E−11	25.56	30
	T9	107.43	48.20	119.70	47.87	160.76	42.89	5.39E−12	29.01	26
DWT	DWT7	939.14	196.4	1528.9	163.3	1110.0	127.5	0.00E+00	271.02	7
	DWT18	10.73	2.99	10.14	3.39	14.91	2.76	3.00E−21	58.07	24
	DWT20	5.06	0.74	4.60	1.55	6.94	0.84	0.00E+00	100.98	17
WPT	WPT1	473.86	98.71	560.73	65.03	775.29	79.45	0.00E+00	284.83	5
	WPT20	2.04	0.26	2.65	0.27	1.67	0.59	0.00E+00	120.83	14
	WPT22	2.50	1.61	2.68	0.41	1.62	0.60	1.85E-10	24.67	31
	WPT23	0.89	0.17	1.11	0.10	0.75	0.23	0.00E+00	88.78	21
	WPT24	0.80	0.21	1.02	0.18	0.56	0.20	0.00E+00	110.20	16
	WPT26	0.92	0.18	1.14	0.11	0.75	0.23	0.00E+00	92.01	19
	WPT28	0.63	0.22	0.85	0.12	0.52	0.17	1.00E−25	75.19	23

2017 JINST 12 P07009

Table 3. Performance measures for the two density classes using selected features.

Classifiers	Test result	Actual		Sensitivity	Specificity	Accuracy
		Fatty	Dense	(%)	(%)	(%)
ANN	Fatty	80	0	98.77	100	99.37
	Dense	1	79			
SVM	Fatty	78	2	98.73	97.53	98.12
	Dense	1	79			
K-NN	Fatty	76	4	96.2	95.06	96.25
	Dense	3	77			
LDA	Fatty	77	3	97.47	96.3	96.87
	Dense	2	78			
NB	Fatty	76	4	97.44	95.12	96.25
	Dense	2	78			

Table 4. Performance measures for three density classes using selected features.

Classifiers	Test result	Actual			Sensitivity	Specificity	Accuracy
		Fatty	Glandular	Dense	(%)	(%)	(%)
	Fatty	79	1	0	97.53	98.75	98.75
ANN	Glandular	1	78	1	96.3	98.125	97.5
	Dense	1	2	77	98.71	99.375	96.25
				Average	97.5133	98.75	97.5
	Fatty	77	3	0	96.25	98.125	96.25
SVM	Glandular	1	77	2	92.77	96.25	96.25
	Dense	2	3	75	97.4	98.75	93.75
				Average	95.4733	97.7083	95.42
	Fatty	75	5	0	97.4	98.75	93.75
K-NN	Glandular	2	73	5	85.88	92.5	91.25
	Dense	0	7	73	93.59	96.875	91.25
				Average	92.29	96.0417	92.08
	Fatty	76	4	0	97.44	98.75	95
LDA	Glandular	1	77	2	89.53	94.37	96.25
	Dense	1	5	74	97.37	98.75	92.5
				Average	94.78	97.29	94.58
	Fatty	76	4	0	92.68	96.25	95
NB	Glandular	4	72	4	87.8	93.75	90
	Dense	2	6	72	94.73	97.5	90
				Average	91.7367	95.8333	91.66

2017 JINST 12 P07009

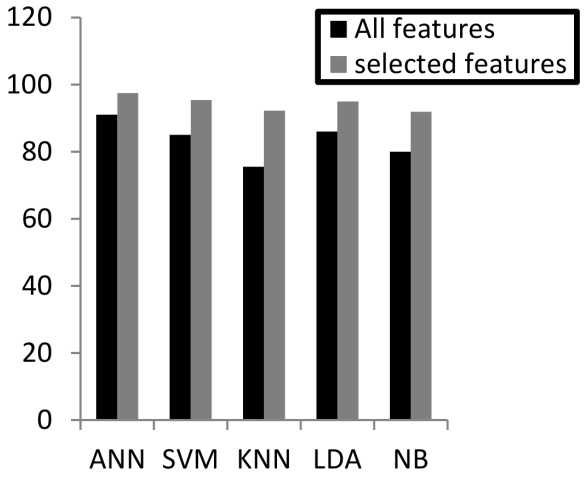

Figure 3. Classification accuracy of five classifiers for three classes (fatty, glandular, and dense).

Table 5. Comparison between fatty/dense and fatty/glandular/dense tissue classification using proposed method with related works which used the MIAS database.

References	Features	Feature selection	Classifier	Two categories accuracy (%)	Three categories accuracy (%)
Proposed	Histogram, GLCM, GLDM, GLRLM, LBP, Gabor, wavelet and trace transform	ANOVA	ANN	99.37	97.5
Sharma et al. [15]	SGLCM, GLDS, FoS ,FPS, law's TEM, Fractal	Fisher's discriminant ratio	KNN	97.22	—
Arefan et al. [13]	Statistical	—	ANN	—	97.66
Abdel-Nasser et al. [14]	Uniform local directional pattern (ULDP)	—	SVM	99	85.5
Sharma et al. [12]	SGLCM, GLDS, FoS, FPS, law's TEM, Fractal	Correlation feature selection	Sequential minimal optimization	96.46	—
Subhashini et al. [9]	Histogram	—	SVM	—	95.44
Mustra et al. [10]	GLCM	Forward and backward feature selection	KNN	91.6	82.5
Oliver et al. [8]	GLCM and Morphological	Sequential feature selection	KNN, NB, Decision tree	91	73

2017 JINST 12 P07009

References

[1] A. Eng et al., *Digital mammographic density and breast cancer risk: a case-control study of six alternative density assessment methods*, *Breast Cancer Res.* **16** (2014) 439.

[2] A. Gubern-Merida et al., *Volumetric breast density estimation from full-field digital mammograms: a validation study*, *PLoS one* **9** (2014) e85952.

[3] M.A. Sak et al., *Current and future methods for measuring breast density: a brief comparative review*, *Breast Cancer Managem.* **4** (2015) 209.

[4] V.A. McCormack and I. dos Santos Silva, *Breast density and parenchymal patterns as markers of breast cancer risk: a meta analysis*, *Cancer EpidemiologyBiomarkers Prev.* **15** (2006) 1159.

[5] L. Ghouti and O. Abdullah, *NMF-density: NMF-based breast density classifier*, ESANN (2014).

[6] American College of Radiology, *Breast Imaging Reporting and Data System (BI-RADS)*, third edition edn, American College of Radiology, Reston U.S.A. (2003).

[7] E.A. Rashed, I.A. Ismail and S.I. Zaki, *Multiresolution mammogram analysis in multilevel decomposition*, *Patt. Recogn. Lett.* **28** (2007) 286.

[8] A. Oliver et al., *A novel breast tissue density classification methodology*, *IEEE Trans. Inf. Technol. Biomed.* **12** (2008) 55.

[9] T. Subashini, V. Ramalingam and S. Palanivel, *Automated assessment of breast tissue density in digital mammograms*, *Comp. Vis. Imag. Underst.* **114** (2010) 33.

[10] M. Mustra, M. Grgic and K. Delac, *Breast density classification using multiple feature selection*, *Automatica* **53** (2012) 362.

[11] N. Vallez et al., *Breast density classification to reduce false positives in CADe systems*, *Comp. Methods Programs Biomed.* **113** (2014) 569.

[12] V.Sharma and S.Singh, *CFS-SMO based classification of breast density using multiple texture models*, *Med. Bio. Eng. Comput.* **52** (2014) 521.

[13] D. Arefan et al., *Automatic breast density classification using neural network*, 2015 *JINST* **10** T12002.

[14] M. Abdel-Nasser et al., *Analysis of tissue abnormality and breast density in mammographic images using a uniform local directional pattern*, *Expert Syst. Appl.* **42** (2015) 9499.

[15] V.Sharma and S.Singh, *Automated classification of fatty and dense mammograms*, *J. Med. Imag. Health Informat.* **5** (2015) 520.

[16] J. Anitha et al., *A dual stage adaptive thresholding for automatic mass detection in mammograms*, *Comput. Methods Programs Biomed.* **138** (2017) 94.

[17] J. Suckling et al., *The mammographic image analysis society digital mammogram database*, *Excerpta Medica, International Congress Series* **1069** (1994) 375.

[18] G. Castellano et al., *Texture analysis of medical images*, *Clinical Radiol.* **59** (2004) 1061.

[19] M. Radovic et al., *Parameter optimization of a computer-aided diagnosis system for detection of masses on digitized mammograms*, **23** (2015) 757.

[20] K. Kalyan et al., *Artificial neural network application in the diagnosis of disease conditions with liver ultrasound images*, *Adv. Bioinf.* (2014) 708279.

[21] S.-H. Peng et al., *Texture feature extraction based on a uniformity estimation method for local brightness and structure in CT images*, *Comput. Biol. Med.* **40** (2010) 931.

2017 JINST 12 P07009

[22] M. Suganthi and M. Madheswaran, *An improved medical decision support system to identify the breast cancer using mammogram*, *J. Med. Syst.* **36** (2012) 79.

[23] U. RajendraAcharya et al., *Ultrasound-based tissue characterization and classification of fatty liver disease: a screening and diagnostic paradigm*, *Knowledge-Based Systems* **75** (2015) 66.

[24] A.P. Singh and B. Singh, *Texture features extraction in mammograms using non-Shannon entropies*, Lecture Notes in Electriaal Engeneering volume 68, Springer (2010).

[25] U. RajendraAcharya et al., *Non-invasive automated 3D thyroid lesion classification in ultrasound: A class of ThyroScan^{TM} systems*, *Ultrasonics* **52** (2012) 508.

[26] Y. Zheng, *Breast cancer detection with Gabor features from digital mammograms*, *Algorithms* **3** (2010) 44.

[27] M. Hussain et al., *Effective extraction of Gabor features for false positive reduction and mass classification in mammography*, *Appl. Math. Inf. Sci.* **8** (2014) 397.

[28] J.Virmani, and V.Kumar, *Prediction of liver cirrhosis based on multiresolution texture descriptors from B-mode ultrasound*, *Int. J. Convergence Computing* **1** (2013) 13.

[29] Y. Zhang et al., *Pathological brain detection in MRI scanning by wavelet packet Tsallis entropy and fuzzy support vector machine*, Springer, Germany (2015).

[30] K. Ganesan et al., *One-class classification of mammograms using trace transform functional*, *IEEE Trans. Instrum. Meas.* **63** (2014) 304.

[31] U.R. Acharya et al., *Application of non-linear and wavelet based features for the automated identification of epileptic EEG signals*, *Int. J. Neural Syst.* **22** (2012) 1250002.

[32] F.Amato et al., *Artificial neural networks in medical diagnosis*, *J. Appl. Biomed.* 11 (2013) 47.

[33] B. Verma and P. Zhang, *A novel neural-genetic algorithm to find the most significant combination of digital mammograms*, *Appl. Soft Comput.* **7** (2007) 612.

[34] M.E. Osman et al., *Computer aided diagnosis system for classification of microcalcifications in digital mammograms*, talk given at the 26th *National Radio Science Conference*, March 17–19, New Cairo, Egypt (2009).

[35] S. Sharma and P. Khanna, *Computer-aided diagnosis of malignant mammograms using Zernike moments and SVM*, *J. Digit. Imaging* **28** (2015) 77.

[36] V. Egorov et al., *Differentiation of benign and malignant breast lesions by mechanical imaging*, *Breast Cancer Res. Treat.* **118** (2009) 67.

[37] S. Mika et al., *Fisher discriminant analysis with kernels*, in the proceedings of *Neural Networks for Signal Processing IX*, August 25, Madisn U.S.A. (1999).

[38] E. Ataer-Cansizoglu et al., *Computer-based image analysis for plus disease diagnosis in retinopathy of prematurity: performance of the "i-ROP" system and image features associated with expert diagnosis*, *Transl. Vis. Sci. Technol.* **4** (2015) 5.

2017 JINST 12 P07009